Monophosphate Tungsten Bronzes. A New Family of Low-Dimensional, Charge-Density-Wave Oxides

MARTHA GREENBLATT

Department of Chemistry, Rutgers, the State University of New Jersey, Piscataway, New Jersey 08855-0939

Received August 15, 1995

Sodium tungsten oxide, Na_xWO_3, was discovered by Wohler in 1824, who called these materials bronzes, because of their metallic luster.[1] The term bronze has been extended to a large variety of reduced ternary transition metal oxides with the general formula $A_xM_yO_z$, and bronzes are known with A as virtually any cation (e.g., alkali, alkaline earth, and rare earth metals) and M as Ti, V, Mn, Nb, Mo, Ta, W, and Re. Binary, reduced transition metal oxides (e.g., Mo_4O_{11}, ReO_3), as well as quaternary and more complex compositions, are often classified as bronzes as well. The structures of these materials are closely related to that of ReO_3 with MO_6 corner- and/or edge-sharing octahedra arranged in three-dimensional (3D) networks, two-dimensional (2D) layer-like structures, or one-dimensional (1D) chain structures; the A cations fill the interstitial sites of the network structure created by the corner/edge-sharing polyhedra. Typically the bronzes are intensely colored with a metallic sheen and chemically inert to even strong acids and exhibit metallic or semiconducting behavior.

There has been continuous interest in the reduced transition metal oxide bronzes for several decades, with a marked increase in research activity starting in the early 1980s with the discovery of charge-density-wave (CDW) phenomena in the first oxide material, the quasi-1D blue bronze, $K_{0.3}MoO_3$.[2] Subsequently, evidence of CDW in the 2D purple molybdenum bronzes ($A_{0.9}Mo_6O_{17}$)[3] and sliding CDW motion in the blue bronzes[4] fueled further interest. Recently, the discovery of multiple CDWs in the 2D monophosphate tungsten bronzes (MPTBs; $(PO_2)_4(WO_3)_{2m}$)[5] provided continued interest in these materials. Moreover, discovery of the high-temperature (T_c) superconducting cuprates with similar low-dimensional (LD) structural and electronic properties raises new questions about the properties of the LD bronzes and their relationship to the high-T_c materials.

In this Account the synthesis and the structure−property relationships in the monophosphate tungsten bronzes will be reviewed. However, since these materials have many structural and physical property features in common with the molybdenum and tungsten bronzes, the latter will be briefly reviewed first.

Martha Greenblatt received her Bachelor's degree from Brooklyn College in Brooklyn, NY, in 1962, and her Ph.D. from the Polytechnic Institute of Brooklyn in 1967. She was a Visiting Scientist at the Weizmann Institute in 1972–1973. She joined the faculty of Rutgers University in July 1974, where she is presently Professor of Chemistry. She spent the summer of 1980 as Visiting Professor at the Clarendon Laboratory, Oxford University, England, and a sabbatical year at Bell Laboratories, Murray Hill, NJ, in 1980–1981. Her research interests are in the area of solid-state chemistry, including the synthesis and characterization of quasi-low-dimensional transition metal compounds, fast ionic motion in solids, and high-temperature superconducting materials.

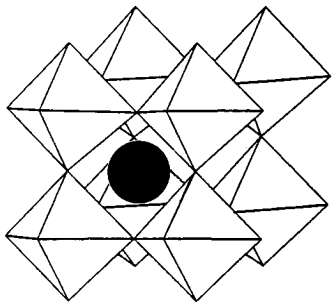

Figure 1. Structure of ReO_3. The solid circle shows the position of the A cation in A_xWO_3.

Tungsten Bronzes

The tungsten bronzes, A_xWO_3, have been investigated continuously since the 1940s, and there are several reviews on the subject that are now more than 20 years old.[6] These materials are fascinating, nonstoichiometric compounds, and although phases with a large variety of A cations have been synthesized, the best-studied compounds are those with A = alkali metal ions. For example, Na_xWO_3 with $0 \leq x \leq 1$ forms a series of solid solutions of sodium metal in WO_3. The structure of WO_3 is similar to that of ReO_3 (Figure 1) and is made up of WO_6 octahedra that corner share in 3D to form a network with large, interconnected, empty cubo-octahedral cavities. The structure of WO_3 is significantly distorted from the ideal representation given in Figure 1 (i.e., in WO_3 the octahedra are tilted and the W−O distances are unequal).[7] The A cations occupy 12 coordinated cubo-octahedral cavities, and at $x = 1$, $NaWO_3$ forms with the ideal, stoichiometric cubic perovskite structure. The color, the structure, and the properties of the bronzes change dramatically with composition. For example, WO_3 is pale-green (the color arises from a small oxygen deficiency, i.e., $WO_{3-\delta}$, that introduces a slight mixed valency of $W^{5+/6+}$), and as x increases for Na_xWO_3, the color changes to gray, blue, purple, red, orange, and finally golden yellow at $x \approx 1$. Single

(1) (a)Wohler, F. *Ann. Phys. Chem. (Pogg. Ann.)* **1924**, *2*, 345. (b)Wohler, F. *Philos. Mag.* **1825**, *66*, 263−268.
(2) Buder, R.; Devenyi, J.; Dumas, J.; Marcus, J.; Mercier, J.; Schlenker, C.; Vincent, H. *J. Phys., Lett.* **1982**, *43*, L59−L63.
(3) Escribe-Filippini, C.; Konate, K.; Marcus, J.; Schlenker, C.; Almairac, R.; Aryloes, R.; Roucau, C. *Philos. Mag.* **1984**, *B50*, 321−330.
(4) Schlenker, C.; Dumas, J. In *Crystal Chemistry and Properties of Materials with Quasi-One-Dimensional Structures*; Rouxel, J., Ed.; Reidel: Dordrecht, The Netherlands, 1986; pp 135−177.
(5) Wang, E.; Greenblatt, M.; Rachidi, I. E.-I.; Canadell, E.; Whangbo, M.-H.; Vadlamannati, S. *Phys. Rev.* **1989**, *B39*, 12969−12972.
(6) (a) Hagenmulller, P. In *Progress in Solid State Chemistry*; Reiss, H., Ed.; Pergamon: New York, 1971; Vol. 5, pp 71−145. (b) Banks, E.; Wold, A. In *Preparative Inorganic Reactions*; Jolly, W. L., Ed.; Interscience: New York, 1968; Vol. 4, pp 237−268.
(7) Wells, A. F. *Structural Inorganic Chemistry*; Oxford University Press: Oxford, 1975; p 506.

0001-4842/96/0129-0219$12.00/0

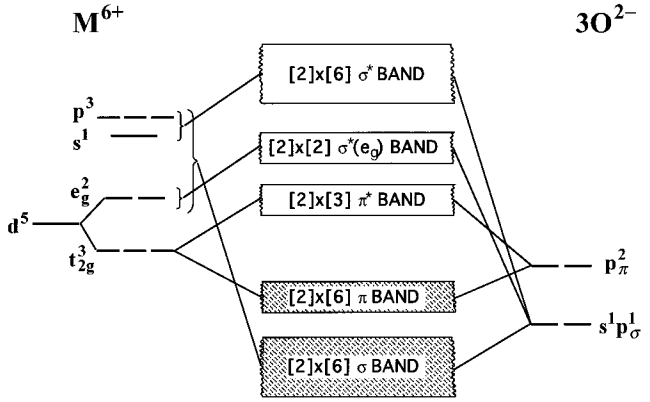

Figure 2. Schematic band structure applicable to the bronzes above the Peierls transition (after ref 9).

crystals of alkali metal A_xWO_3 can be prepared easily by fused-salt electrolysis, and they are some of the most beautiful, intensely colored synthetic materials.[8] Equally intriguing is the electrical conductivity of the tungsten bronzes. WO_3 is an insulator, but for Na_xWO_3, the electrical conductivity increases with increasing x, and at $x \geq 0.28$ the deeply colored materials change from semiconducting to metallic in behavior.

The electronic properties of the tungsten bronzes (or those of any bronze) can be understood by the simple schematic band diagram shown in Figure 2, which was first proposed by Goodenough.[9] In this model each oxygen forms sp hybrids directed toward neighboring tungsten atoms. The central tungsten atoms with 6s, 6p, and 5d (e_g) orbitals overlap with the sp hybrids of oxygens to form σ and σ^* bands. Similarly, the W 5d t_{2g} orbitals mix with the oxygen pπ orbitals to form π and π^* bands. The levels are filled up to and including the pπ level with the 24 electrons of WO_3. The conduction band, the π^* band of W 5d t_{2g} parentage is empty, and WO_3 is an insulator, because the band gap is ~3 eV. In A_xWO_3, the A cations donate their electrons into the conduction band, partially filling it and accounting for the metallic behavior (or to levels just below the bottom of the conduction band, in which case the material is semiconducting, e.g., $A_{0.33}MoO_3$).

Molybdenum Bronzes

The first unambiguous report of the synthesis of alkali metal molybdenum bronzes was that of Wold et al., by electrolytic reduction of $A_2MoO_4-MoO_3$ melts, in the early 1960s.[10] These bronzes have been investigated intensively in recent years, because of their unusual properties, which include quasi-low-dimensional behavior, CDW-driven metal-to-insulator transition (MIT), sliding charge-density waves, and insulator-to-superconductor transition. Several recent reviews have been published on these topics.[4,11] The molybdenum bronzes form three different stoichiometric compositions and structure types: the blue bronzes, $A_{0.3}MoO_3$ (A = K, Rb, Tl), which are quasi-1D metals (σ(RT) $\approx 10^4$ $(\Omega\ cm)^{-1}$ (refs 4 and 11); the red bronzes, $A_{0.33}MoO_3$ (A = Li, Na, K, Rb, Cs, Tl), which are semiconducting (σ(RT) $\approx 10^{-4}$ $(\Omega\ cm)^{-1}$) (ref 11a); and the purple bronzes, $A_{0.9}Mo_6O_{17}$ (A = Li, Na, K) and AMo_6O_{17} (A = Tl), which are quasi-2D metals (σ(RT) $\approx 10^4$ $(\Omega\ cm)^{-1}$ (refs 4 and 11). Because of the highly anisotropic structure of these phases, the physical properties and anomalous behavior are best understood when oriented single-crystal data are available. Thus, for all the physical characterizations relatively large (several cubic millimeters in size) single crystals are desirable. Such crystals have been grown for all of the known molybdenum bronze phases by a so-called gradient flux technique.[12]

Charge-Density-Wave State

The blue bronzes undergo a MIT at 180 K.[11] This transition has been attributed to a coupled instability of the conduction electrons and phonons at $2\mathbf{k}_F$ (where $\mathbf{k}_F$ is the Fermi wave vector $\mathbf{q}$, or reciprocal unit cell dimension for the 1D metal), which below a critical temperature (T_c) leads to a modulation of the charge density coupled to a lattice distortion, and an opening of a gap at the Fermi surface (FS) (Figure 3a,b). This response is a consequence of large parallel areas on the FS separated by $2\mathbf{k}_F$ as shown in Figure 3c for the 1D simplest case, where the FS reduces to two infinite parallel planes. This coincidence of one part of the FS with another by mere translation of a wave vector, $\mathbf{q} = 2\mathbf{k}_F$ (for the 1D case), is referred to as nesting. The corresponding periodically modulated electronic density, called the CDW, is $\rho(x) = \rho_0 + \rho_1 \cos(2\mathbf{k}_F x + \phi)$, where ρ_1 is the amplitude and ϕ is the phase of the CDW. The CDW state is said to be commensurate when the period of the CDW is a rational multiple of the crystallographic unit cell. When the period of the CDW and the lattice are irrational, the CDW is said to be incommensurate and the whole sample is the unit cell. The idea that the electronic energy of a 1D metal can be lowered by a CDW was first predicted independently by Peierls[14] (referred to as the Peierls transition) and Fröhlich.[15] The CDW is in principle free to move, and the sliding will carry a current: this was the mechanism for superconductivity proposed by Fröhlich in 1954.[15] In real crystals, the incommensurate CDW is pinned by crystal defects (e.g., impurities and imperfections). However, above a finite threshold electric field (typically a few hundred millivolts), the CDW is depinned and the sliding CDW gives rise to an excess conductivity, the so-called Fröhlich conductivity. The sliding of CDW was first reported by Monceau et al. for $NbSe_3$ nearly 20 years ago.[16] Dumas et al. established that the blue bronze shows nonlinear transport, due to the sliding of the CDW.[17] Subsequent work has shown

(8) (a)Wold, A.; Bellevance, D. In *Preparative Methods in Solid State Chemistry*; Hagenmuller, P., Ed.; Academic Press: New York, 1977; pp 279−308 and references cited therein. (b) Shanks, H. R. *J. Cryst. Growth* **1972**, *13/14*, 433−37.

(9) (a) Goodenough, J. B. *Bull. Soc. Chim. Fr.* **1965**, 1200. (b) Goodenough, J. B. *Czech. J. Phys.* **1967**, *B17*, 304. (c) Dickens, P. G.; Neild, D. *J. Trans. Faraday Soc.* **1968**, *64*, 13−20.

(10) Wold, A.; Kunnmann, W.; Arnott, R. J.; Ferretti, R. J. *Inorg. Chem.* **1964**, *3*, 545−548.

(11) (a) Greenblatt, M. *Chem. Rev.* **1988**, *88*, 31−53. (b) *Low-Dimensional Electronic Properties of Molybdenum Bronzes and Oxides*; Schlenker, C., Ed.; Kluwer: Dordrecht, The Netherlands, 1989; pp 1−448.

(12) McCarroll, W. H.; Greenblatt, M. *J. Solid State Chem.* **1984**, *54*, 282−290.

(13) Grüner, G. *Density Waves in Solids*; Addison-Wesley Publishing Co.: Reading, MA, 1994.

(14) Peierls, R. E. *Quantum Theory of Solids*; Clarendon: Oxford, 1955; p 108.

(15) Fröhlich, H. *Proc. R. Soc. London* **1954**, *A223*, 296.

(16) Monceau, P.; Ong, N. P.; Portis, A. M.; Meerschaut, A.; Rouxel, J. *Phys. Rev. Lett.* **1976**, *37*, 602.

(17) Dumas, J.; Schlenker, C.; Markus, J.; Buder, R. *Phys. Rev. Lett.* **1983**, *50*, 757.

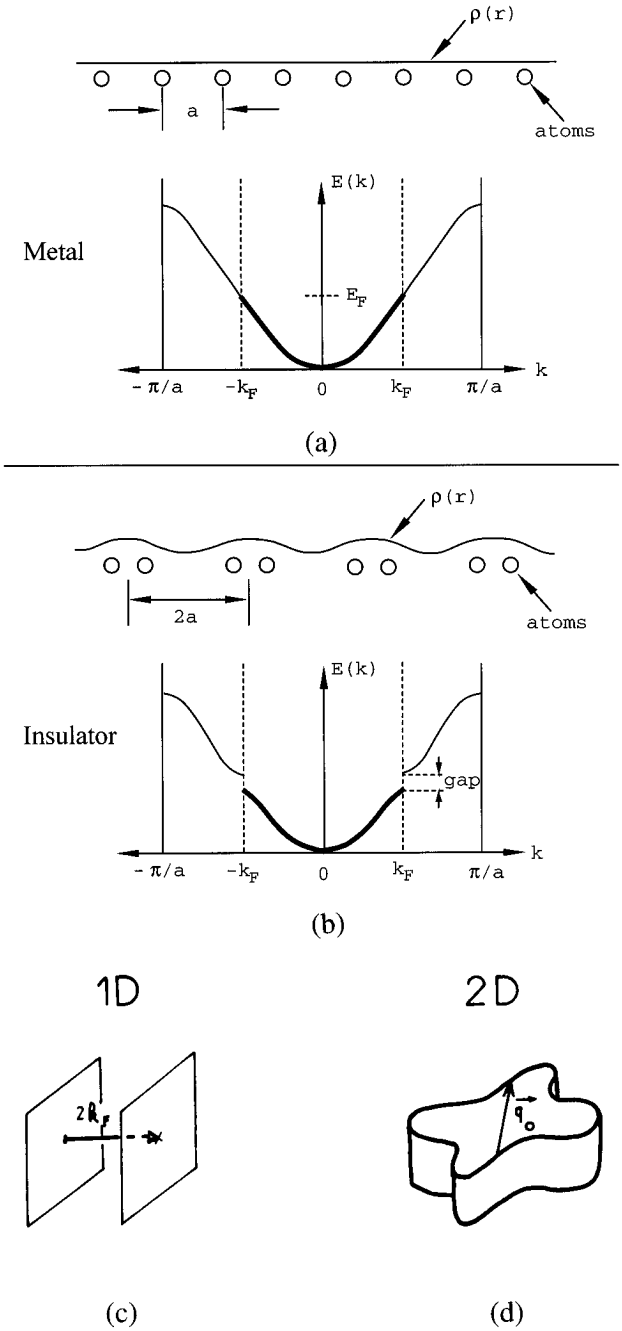

Figure 3. Peierls distortion in a 1D metal with a half-filled band. (a) Undistorted metal (after ref 13). (b) Peierls insulator with period doubling (after ref 13). (c) Fermi surface of a 1D metal and nesting at $\mathbf{q} = 2\mathbf{k}_F$. (d) Fermi surface of a 2D metal and nesting at $\mathbf{q} = \mathbf{q}_0$. Parts c and d are reprinted with permission from ref 11b, p 89. Copyright 1989 Kluwer Academic Publishers.

that the CDW state is not restricted to 1D systems. In contrast to quasi-1D metals, where the gap opening at the FS is normally complete and the Peierls transition is a metal−insulator one, in quasi-2D metals the opening of a gap over the FS is only partial, and a metal−metal transition (MMT) is observed. Indeed the MMT observed in the purple bronzes, $A_{0.9}Mo_6O_{17}$, near 80 and 120 K for A = Na and K or Tl, respectively, is due to the condensation of a CDW state.[11] In an ideal 2D metal the FS is an infinite cylinder with an axis perpendicular to the plane of the layers (Figure 3d). While the nesting between the two planes is perfect in the 1D case, it is only partial between parallel portions of the FS in the 2D case; Figure 3d shows the vector $\mathbf{q}_0$, which nests portions of the cylindrical FS with a similar curvature.

If electron−electron interactions, such as on-site electron−electron repulsions, are important in a LD metal, the ground state may be spin modulated, or a spin-density-wave (SDW) state, rather than a CDW. In this case, below T_c, the spin density for the 1D case, given by $S(x) = 2|S| \cos(2\mathbf{k}_F x + \phi)$ is spatially varying, or a static, spatially varying magnetization, and therefore a spatially dependent magnetic moment develops. As for the CDW, transition to a SDW ground state opens up a gap at the FS, leading to a MIT, which can be either commensurate or incommensurate with the lattice.[13] SDW instabilities may be induced in LD metals by an applied magnetic field as well as by lowering the temperature.[18]

Electron−phonon interactions in a metal can also lead to a superconducting state below T_c. As described by the BCS theory (for Bardeen, Cooper, and Schrieffer, who in 1957 received the Nobel prize in physics for explaining the mechanism of superconductivity), electron−phonon interactions in a metal can lead to the formation of electron pairs, so-called Cooper pairs (these collectively move through the lattice without resistance (R); hence, below T_c, $R = 0$ for the metal), and the opening of a gap at the FS.[19] The BCS gap, Δ ($2\Delta = 3.52 k_B T_c$, where k_B is the Boltzman constant), has a similar form for the CDW, SDW, and superconducting ground states.[13] The CDW, SDW, and superconductivity are always found near a metal−insulator instability. Which of these states occurs depends on the detailed nature of electron−phonon and electron−electron interactions and at present cannot be predicted on the basis of fundamental materials properties.

Of interest and potentially fundamental importance is the observation of a MIT at 24 K, followed by a transition to superconductivity at 2 K in $Li_{0.9}Mo_6O_{17}$ quasi-1D purple bronze.[20] It would be desirable to establish the exact nature of the MIT at 24 K. That is, is it a CDW or SDW or a transition of some other nature? Should either the CDW or SDW coexist with superconductivity in this material, it might help to understand why in some materials the MIT leads to superconductivity and in others to a CDW or SDW state.

Although a CDW-driven phase transition results in anomalies, for example, in the temperature dependence of resistivity and magnetic susceptibility, unambiguous evidence for the CDW sate is the observation of superlattice reflections by diffraction methods, which confirm the distortion of the lattice. X-ray and neutron diffraction studies have demonstrated conclusively that the 180 K transition in the blue bronzes is a Peierls transition to an incommensurate CDW insulating state.[21] Similarly, diffraction studies have confirmed that the transition seen in the purple bronzes is to a $2a^* \times 2b^* \times c^*$, commensurate, CDW state.[3] Analogously, unambiguous evidence for the modulation of the magnetic spin structure in the SDW

(18) See for example: (a) Montambaux, G. In *Low Dimensional Conductors and Superconductors*; Jerome, D., Caron, L. G., Eds.; NATO-ASI Series B: Physics; Plenum: New York, 1987; Vol. 155, pp 233−242. (b) Heritier, M. *Ibid.*; pp 243−252.

(19) Bardeen, J.; Cooper, L. N.; Schrieffer, J. R. *Phys. Rev.* **1957**, *106*, 162.

(20) Greenblatt, M.; McCarroll, W. H.; Neifeld, R.; Croft, M.; Waszczak, J. V. *Solid State Commun.* **1984**, *51*, 671−674.

(21) Pouget, J. P.; Kagoshima, S.; Schlenker, C. *J. Phys. Rev. Lett.* **1983**, *4*, L113−L120.

state is observation of the condensation of magnetic superlattice reflections by temperature dependent neutron diffraction studies.

The highly anisotropic and unusual behavior of the Mo bronzes is attributed to their quasi-LD structures. In contrast to the W bronzes, which have simple 3D perovskite-related structures (see above), the Mo bronzes have complex, layered-like structures of edge- and corner-sharing MO_6 octahedra forming infinite, 2D sheets, which are held together by the A cations (with the exception of the Li phases, which are 3D).[11] Although the structure of the molybdenum bronzes is layer-like, the bonding in these materials is three-dimensional. The quasi-LD character is determined by the location of the unpaired electrons in the structure, and these are delocalized in a highly 1D or 2D directional manner in the bronzes. The anisotropic distribution of conduction electrons is indicated empirically by the bond-valence-sum analysis, which allows one to estimate the oxidation state of a metal from the metal−oxygen distances obtained from structure analysis.[22] Such calculations for $K_{0.3}MoO_3$,[23] $K_{0.9}Mo_6O_{17}$,[24] $Li_{0.9}Mo_6O_{17}$,[25] and Mo_4O_{11}[26] show, for example, that the d-electrons are located on only certain MoO_6 octahedra in the Mo layers, and this imparts the quasi-1D properties of the $K_{0.3}MoO_3$ and $Li_{0.9}Mo_6O_{17}$ and similarly the quasi-2D properties of $K_{0.9}Mo_6O_{17}$ and Mo_4O_{11}. This highly anisotropic delocalization of the d-electrons, predicted by the bond-valence analysis, is confirmed by band structure calculations.[27]

Phosphate Tungsten Bronzes (PTBs)

In the past 10 years, Raveau and his group have synthesized a very large number of reduced ternary and quaternary transition metal phosphate compounds, $A_xP_yM_zO_w$ with M = Ti, V, Nb, Mo, and W, where some of the MO_6 octahedra in the ReO_3-type slabs are replaced in an ordered fashion by either monophosphate, PO_4, or diphosphate, P_2O_7, groups. Recently overviews of the structural properties of the Ti, V, Nb, Mo, and W phosphate bronzes have been published.[28] Some of these materials, particularly the phosphate tungsten phases (i.e., M = W) show bronze-like behavior including intense color, metallic sheen, and high electronic conductivity.

Three major structural classes of phosphate tungsten bronzes have been discovered in the course of their synthesis: the monophosphate tungsten bronzes with pentagonal tunnels ($MPTB_p$s) have the general formula $(PO_2)_4(WO_3)_{2m}$;[29] the monophosphate bronzes with hexagonal tunnels ($MPTB_h$s) have the general formula $A_x(PO_2)_4(WO_3)_{2m}$ with A = Na or K;[30] and diphosphate tungsten bronzes (DPTBs) have the general formula $A_x(P_2O_4)_2(WO_3)_{2m}$ where A = K, Rb, Tl, and Ba.[31] Recently the structural and physical properties of all of the PTBs have been reviewed in detail.[32] In this Account an overview of the structure−property relationships of the MPTBs will be reviewed.

Monophosphate Tungsten Bronzes with Pentagonal Tunnels

Structural Properties. The homologous series, with the general formula $(PO_2)_4(WO_3)_{2m}$ where m is an integer (2, 4−16), represent the family of $MPTB_p$s.[29] In addition, $A_x(PO_2)_4(WO_3)_{2m}$ with A = Na and K, $x < 1$, also form with this structure. The structure of these bronzes can be described by the stacking, along the orthorhombic [001] direction, of ReO_3-type slabs of corner-sharing WO_6 octahedra; the slabs are connected by corner-sharing with PO_4 tetrahedra, forming layers in the *ab* plane of the orthorhombic unit cell (Figure 4). Note that the string of octahedra from one slab to the next are related by 180° and run in a zigzag fashion. At the juncture between two ReO_3-type slabs, corner-sharing octahedra and tetrahedra form pentagonal tunnels, which are empty in the $(PO_2)_4(WO_3)_{2m}$ phases, but may be occupied partially by the smaller alkali metal ions in $A_x(PO_2)_4(WO_3)_{2m}$ [(Na, K), (Na, Li), (K, Na); $x < 1$].[33] The value of m determines the width of the ReO_3-type slabs. For even-m members the number of WO_6 octahedra in the slabs is $m/2$ (Figure 3a, $m = 2$; Figure 3b, $m = 4, 6, 8$), while for odd-m members there are $(m + 1)/2$ and $(m - 1)/2$ strings of octahedra alternating in adjacent ReO_3-type slabs that repeat in a zigzag fashion (Figure 3c, $m = 5, 7, 9$). The a and b lattice parameters are almost independent of m ($a \cong 5.3$ and $b \cong 6.6$ Å), while c varies according to the empirical formula $c \cong (4.9 + 3.1m)$ Å.[29f] The $m = 6$ member of the $MPTB_p$ family is isostructural with γ-Mo_4O_{11}, with PO_4 replacing the MoO_4 tetrahedra and, of course, WO_6 octahedra replacing the MoO_6 octahedra.[29c]

In addition to the empty pentagonal tunnels, there are empty cubo-octahedral cavities in the ReO_3-like slabs of the MPTBs. This structural feature and the mixed valency of W (W^{VI}/W^{V}) suggested that lithium and/or sodium ions might be electrochemically and reversibly inserted into these phases for possible applications as cathode materials in secondary batteries and related electrochemical devices. Reactions of MPTBs with *n*-butyllithium and sodium naphthalide, respectively, indicated that, indeed, two Li ions and ∼1 Na ion per W may be inserted into various MPTBs.[33]

Measurement of the electrical transport and magnetic properties of polycrystalline $MPTB_p$, by Benmoussa et al., indicated metallic behavior.[34] The mixed valency of the ReO_3-type tungsten oxide layers and the separation of these presumably conducting layers by insulating phosphate "planes" predicted 2D

(22) (a) Zachariasen, W. H. *J. Less-Common Met.* **1978**, *61*, 1. (b) Brown, D. In *Structure and Bonding in Crystals II*; O'Keefe, M., Navrotsky, A., Eds.; Academic Press: New York, 1981; pp 1−30.
(23) Vincent, H.; Marezio, M. Reference 11b, pp 49−85.
(24) Vincent, H.; Ghedira, M.; Marcus, J.; Mercier, J.; Schlenker, C. *J. Solid State Chem.* **1983**, *47*, 113−121.
(25) Onoda, M.; Toriumi, K.; Matsuda, Y.; Sato, M. *J. Solid State Chem.* **1987**, *66*, 163−170.
(26) Onoda, M.; Fujishita, H.; Matsuda, Y.; Sato, M. *Synth. Met.* **1987**, *19*, 947.
(27) Canadell, E.; Whangbo, M.-H. *Chem. Rev.* **1991**, *91*, 965−1034.
(28) (a) Raveau, B. *Proc. Indian Natl. Sci. Acad.* **1986**, *A52*, 67−101. (b) Borel, M. M.; Goreaud, M.; Grandin, A.; Labbe, Ph.; Leclaire, A.; Raveau, B. *Eur. J. Solid State Inorg. Chem.* **1991**, *28*, 93−129.
(29) (a) Giroult, J. P.; Goreaud, M.; Labbe, Ph.; Raveau, B. *Acta Crystallogr.* **1981**, *B37*, 2139−2142. (b) Benmoussa, A.; Labbe, Ph.; Groult, D.; Raveau, B. *J. Solid State Chem.* **1982**, *44*, 318−324. (c) Labbe, Ph.; Goreaud, M.; Raveau, B. *J. Solid State Chem.* **1986**, *61*, 324−331. (d) Wang, S. L.; Wang, C. C.; Lii, K. H. *J. Solid State Chem.* **1989**, *82*, 298−302. (e) Domenges, B.; Hervieu, M.; Tilley, R. J. D.; Raveau, B. *J. Solid State Chem.* **1984**, *54*, 10−28. (f) Domenges, B.; Studer, F.; Raveau, B. *Mater. Res. Bull.* **1983**, *18*, 669−676.
(30) Lamire, M.; Labbe, Ph.; Goroud, M.; Raveau, B. *J. Solid State Chem.* **1987**, *66*, 64−72.
(31) Lamire, M.; Labbe, Ph.; Goreaud, M.; Raveau, B. *J. Solid State Chem.* **1987**, *71*, 342−348.
(32) Greenblatt, M. *Int. J. Mod. Phys.* **1993**, *B7*, 3937−3971.
(33) Wang, E.; Greenblatt, M. *J. Solid State Chem.* **1987**, *68*, 38−44.
(34) Benmoussa, A.; Groult, D.; Raveau, B. *Rev. Chim. Miner.* **1984**, *21*, 710−720.

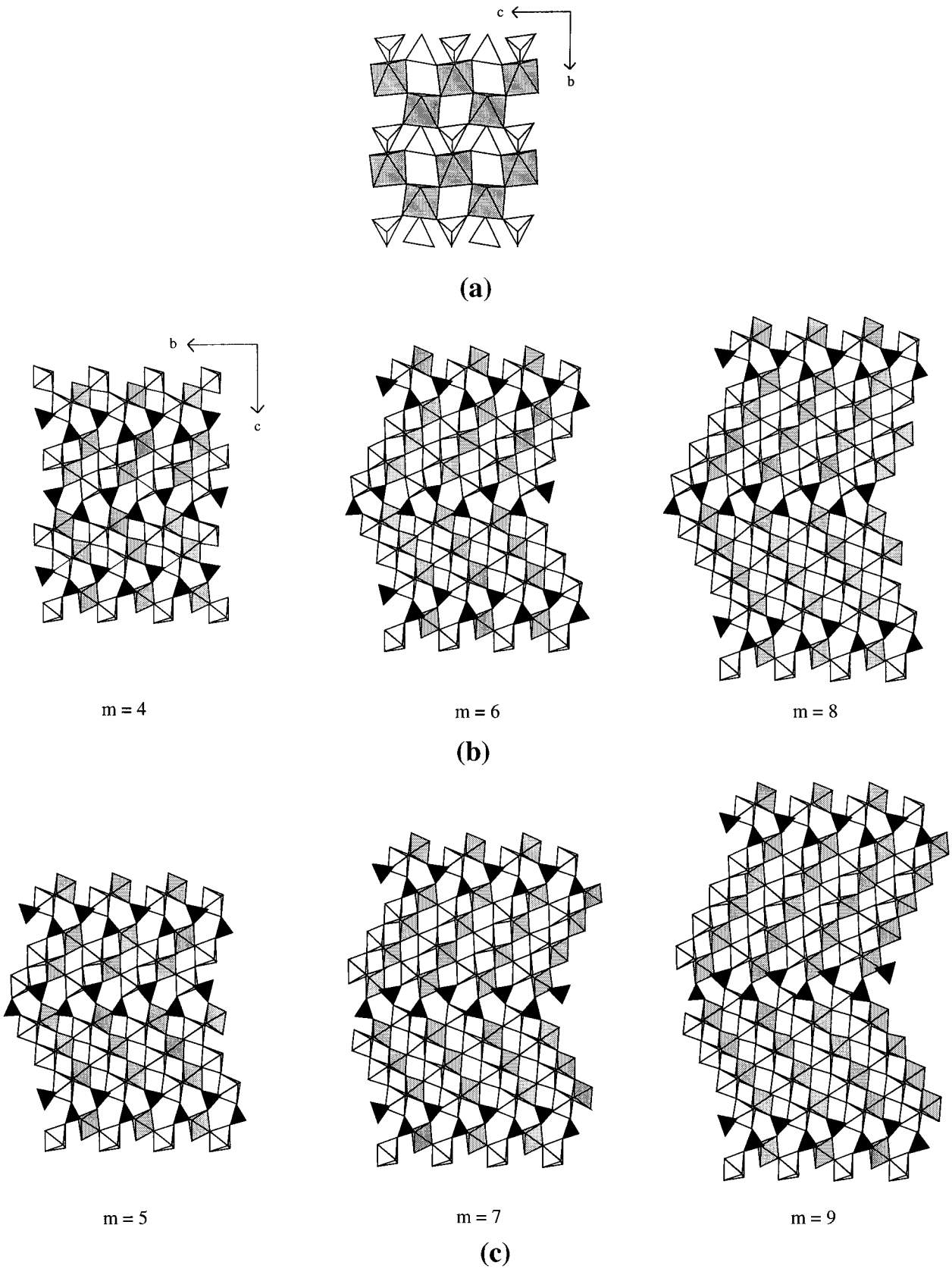

Figure 4. Schematic structure of the monophosphate tungsten bronzes ($MPTB_p$s), $(PO_2)_4(WO_3)_{2m}$; (a) $m = 2$ showing zigzag chains of WO_6 octahedra separated by PO_4 tetrahedra; (b) $m = 4$, 6, and 8; (c) $m = 5$, 7, and 9 with $m/2$-wide slabs of ReO_3-type WO_6 octahedra interconnected by PO_4 tetrahedra.

properties for the $MPTB_p$s. Moreover, the thickness of the ReO_3-type blocks and therefore the *c* unit cell parameter increase with *m* (Table 1), whereas *a* and *b* are only weakly dependent on *m*. However, the number of 5d-electrons per unit cell is independent of *m*, and is always 2 (except when A cations are inserted into the cavities). Thus, because the low dimensionality depends on the width of the ReO_3-type slabs, these

Table 1. Variations of the *c* Parameter with *m* for the Series of $(PO_2)_4(WO_3)_{2m}$ Single Crystals and Their Oxidation States (*n*+), Room Temperature Resistivities (ρ(RT)), and Transition Temperatures (T_{c1} and T_{c2})

compound	m	*n*+	*c* (Å)	ρ(RT) (Ω cm)	T_{c1}[a] (K)	T_{c2}[a] (K)
PWO_5	2	5	11.199(3)	$\sim10^{-3}$		
$P_4W_8O_{32}$	4	5.5	17.383(1)	$\leq10^{-4}$	~85 (80)	60 (52)
$P_4W_{12}O_{44}$	6	5.67	23.560(2)	$\sim10^{-4}$	~114 (120)	60 (52)
$P_4W_{14}O_{50}$	7	5.71	26.631(4)	$\sim10^{-2}$	~180 (188)	47 (60)
$P_4W_{16}O_{56}$	8	5.75	29.722(3)	$\sim10^{-3}$	(220)	(200)
$P_4W_{18}O_{62}$	9	5.78	32.800(15)[b]	$\sim10^{-3}$	(~445)	(324)
$P_4W_{20}O_{68}$	10	5.80	35.952(14)[b]	$\sim10^{-3}$	>RT	
$P_4W_{24}O_{80}$	12	5.83	42.1[c]	$\sim10^{-2}$	>RT	
$P_4W_{28}O_{92}$	14	5.86	48.3[c]		>RT	

[a] Values in parentheses are from X-ray diffuse scattering experiments. [b] From HREM experiments, ref 28e. [c] Calculated using $c = (4.9 + 3.1m)$, ref 27.

materials are excellent models for studying the effect of dimensionality on the properties, without changing the electron count.

Synthesis and Crystal Growth. Typically the compounds can be synthesized in polycrystalline form by a two-step process. In all cases a mixture of ammonium hydrogen phosphate, $(NH_4)_2HPO_4$, and WO_3 (and alkali metal carbonate in the A−P−W−O compositions) is heated at ~650 °C to decompose the phosphate (carbonate). The product of this decomposition reaction is mixed with the appropriate amount of tungsten and heated in an evacuated quartz tube for prolonged periods at >1000 °C.[29,30] This method of synthesis often also yields small single crystals, which are large enough for single-crystal X-ray structure analysis, but too small for physical measurements. Platelike single crystals of $MPTB_p$, suitable for physical measurements (~2−3 × 0.5−1 × 0.2−1 mm^3), with $m = 2$, 4, 6, 7, and 8, have been grown by chemical vapor transport in a two-zone horizontal furnace from stoichiometric quantities of the starting materials in evacuated quartz tubes with various transporting agents. The optimal temperature conditions and transporting agents required for each system were determined empirically, and details of the synthesis have been published. Crystals of PWO_5 ($m = 2$) are dark-brown,[35] $P_4W_8O_{32}$ ($m = 4$) are purple,[36] and $P_4W_{12}O_{44}$ ($m = 6$),[5] $P_4W_{14}O_{50}$ ($m = 7$),[37] $P_4W_{16}O_{56}$ ($m = 8$),[38] $P_4W_{20}O_{68}$ ($m = 10$),[39] and $P_4W_{24}O_{80}$ ($m = 12$)[40] are dark-blue bronzes.

Electrical and Magnetic Properties. X-ray oriented single crystals were used to measure the anisotropic electrical and magnetic behavior of each phase. Figures 5−8 show the resistivity as a function of temperature of $m = 2$ (ref 35), 6 (ref 5), 7 (ref 41), and 8 (ref 38), respectively.

PWO_5, the $m = 2$ phase, is highly anisotropic; it has high conductivity at room temperature (RT) (ρ(RT) ≈ 10^{-3} Ω cm) along the *c* direction (Figure 5), and the conductivity is an order of magnitude lower along the other crystallographic directions. However, the temperature variation of the conductivity is indicative of semiconducting behavior. The magnetic susceptibility shows Curie−Weiss behavior (Figure 9) and antiferromagnetic ordering at low temperature (~15 K).[35] The structure of this member has single chains of isolated, corner-sharing WO_6 octahedra separated by PO_4 tetrahedra (Figure 4a), so one might expect quasi-1D behavior.[29d] Band structure calculations predict both metallic and magnetic behavior in partially filled dispersive and flat bands along the direction of the WO_6 chains.[27] It is possible that this material under-

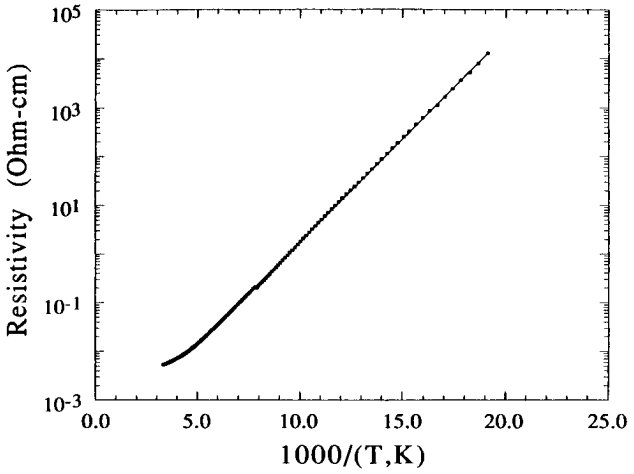

Figure 5. Temperature dependence of the resistivity for PWO_5, the $m = 2$ MPTB, for current along the *c* axis (easy axis of conductivity). Reprinted with permission from ref 35. Copyright 1991 Academic Press.

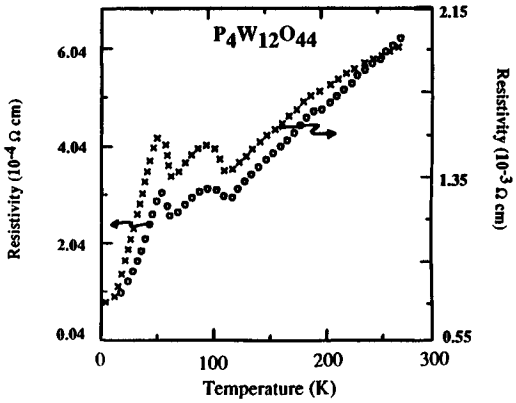

Figure 6. Temperature dependence of the resistivity for $P_4W_{12}O_{44}$, the $m = 6$ member, for current along the *c* axis (hard axis (×)) and in the *ab* plane (easy axis (○)). Reprinted with permission from ref 5. Copyright 1989 American Institute of Physics.

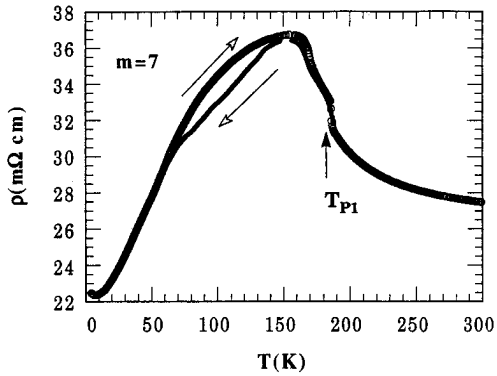

Figure 7. Temperature dependence of the resistivity for $P_4W_{14}O_{50}$, the $m = 7$ member, for current in the *ab* plane (easy axis; heating/cooling cycles).

(35) Teweldemedhin, Z. S.; Ramanujachary, K. V.; Greenblatt, M. *J. Solid State Chem.* **1991**, *95*, 21−28.
(36) Teweldemedhin, Z. S.; Ramanujachary, K. V.; Greenblatt, M. *Phys. Rev.* **1992**, *B46*, 7897−7900.
(37) Teweldemedhin, Z. S.; Greenblatt, M. To be published.
(38) Teweldemedhin, Z. S.; Greenblatt, M. To be published.
(39) Goroud et al. To be published.
(40) Schlenker, C.; LeTouze, C.; Hess, C.; Rötger, A.; Dumas, J.; Marcus, J.; Greenblatt, M.; Teweldemedhin, Z. A.; Ottolenghi, A.; Foury, P.; Pouget, J. P. *Synth. Met.* **1995**, *70*, 1263−1266.

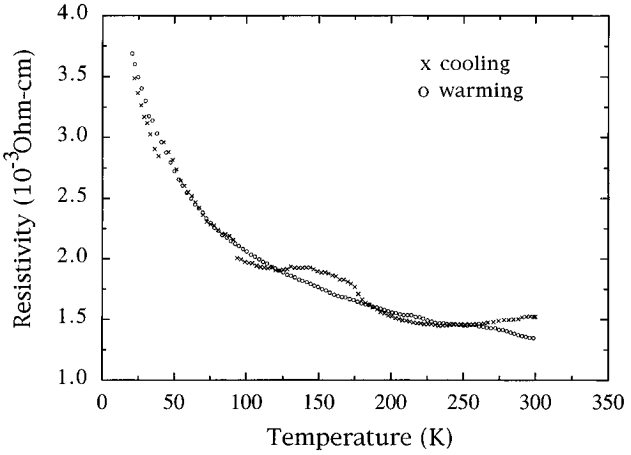

Figure 8. Temperature dependence of the resistivity for $P_4W_{16}O_{56}$, the $m = 8$ member, for current in the *ab* plane (easy axis; heating/cooling cycles).

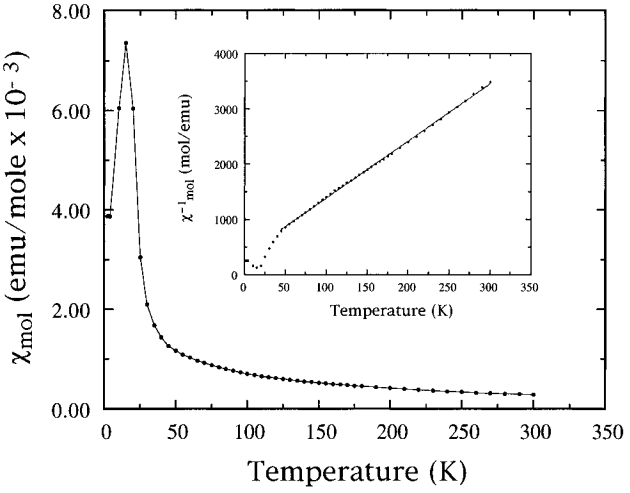

Figure 9. Temperature dependence of the magnetic susceptibility for PWO_5 on a batch of single crystals oriented almost along the *c* axis. Reprinted with permission from ref 35. Copyright 1991 Academic Press.

goes a CDW transition at higher temperatures (ρ was measured in the range of 10−390 K). The $m = 4$ and 6 members show anisotropic, metallic transport properties with the electrical conductivity (σ) at least an order of magnitude higher in the *ab* plane than along the *c* direction for each system, as predicted by the 2D structural properties. Two giant anomalies are evident in the resistivity data at $T_{c1} \approx 85$ K and $T_{c2} = 60$ K and $T_{c1} \approx 114$ K and $T_{c2} = 60$ K for the $m = 4$ and 6 members, respectively (see Figure 6 for $m = 6$; Table 1), which suggest transitions to two CDW states in each. The temperature dependence of magnetic susceptibility shows similar 2D properties and large drops in the magnetic susceptibility (Figure 10 for the $m = 6$ member) at temperatures where anomalies are seen in the resistivity data for each compound.[5,36] The $m = 7$ member has unique transport behavior, and it shows several anomalies in the ρ vs T data (Figure 7); it is metallic at RT and undergoes a MMT at $T_{c1} \approx$ 180 K, another MMT at $T_{c2} = 170$ K, and a third one at $T_{c3} = 47$ K.[37,41] The magnetic susceptibility of this phase does not show anomalies at the temperatures seen in the resistivity data. The ρ vs T data of the $m = 8$ phase show semiconducting behavior of the

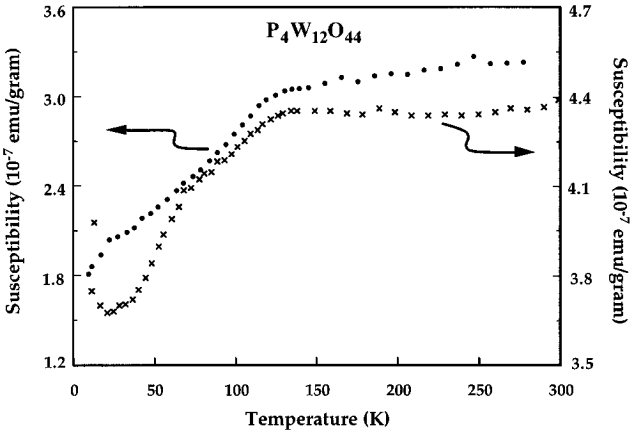

Figure 10. Temperature dependence of the magnetic susceptibility for a batch of oriented single crystals of $P_4W_{12}O_{44}$. The applied magnetic field ($\mathbf{H} = 1$ T) is parallel with the *c* axis (hard (×)) and in the *ab* plane (easy (○)). Reprinted with permission from ref 5. Copyright 1989 American Institute of Physics.

resistivity as a function of temperature; $\rho(\text{RT}) \approx 10^{-3}$ Ω cm in the *ab* plane and ∼15−20 Ω cm along the *c* direction, an enormous anisotropy. There is a hump-like anomaly in the range of 120−200 °C (Figure 8). The transport properties are consistent with the Curie−Weiss behavior of the temperature dependence of the magnetic susceptibility from room temperature down to 2 K. Preliminary results of the temperature dependence of the resistivity have been obtained on the $m = 10$ and $m = 12$ members. Several electronic instabilities are evident in each case.[40]

Band structure calculations by Canadell and Whangbo using a tight binding extended Hückel (EHTB) method lead to three bands crossing the Fermi level for $P_4W_8O_{32}$ ($m = 4$)[27] and $P_4W_{12}O_{44}$ ($m = 6$)[5,27] as shown in Figure 11a for $P_4W_{12}O_{44}$. With two electrons to fill the bottom three bands, the FSs calculated for the $m = 6$ member are shown in Figure 11b, where the shaded and unshaded regions represent the filled and empty band levels, respectively. To show the nesting among the three FSs, they are combined in Figure 11c. The representation of FS nesting behavior shown in Figure 11c is quite general for all the MPTBs with minor changes for different values of *m*. Canadell and Whangbo have shown that the combined FSs in Figure 11c can be decomposed into three sets of hidden 1D FSs as shown in Figure 11d for an ideal case.[42] Moreover, each of the three quasi-1D FSs is associated with infinite chains of WO_6 octahedra in the *a* and $a \pm b$ directions of the ReO_3-like slabs found in $P_4W_{12}O_{44}$.[43]

Investigations of X-ray diffuse scattering (XRDS) by Pouget on the $m = 4$ (ref 43), 6 (ref 43), 7 (ref 43), and 8, 9, 10, 12, and 14 (refs 43−45) members of $MPTB_p$ at ambient temperature give further evidence for quasi-1D CDW fluctuations. For all of the MPTB studied, these fluctuations condense into two and in some cases three successive structural phase transitions at about the same temperature where the electrical resistivity shows large anomalies confirming

(41) Rötger, A.; Schlenker, C.; Dumas, J.; Wang, E.; Teweldemedhin, Z.; Greenblatt, M. *Synth. Met.* **1993**, *55−57*, 2670−2675.

(42) Canadell, E.; Whangbo, M.-H. *Int. J. Mod. Phys. B* **1993**, *7*, 4005−4043.

(43) Foury, P.; Pouget, J. P. *Int. J. Mod. Phys. B* **1993**, *7*, 3973−4003.

(44) Foury, P.; Pouget, J. P.; Teweldemedhin, Z. S.; Wang, E.; Greenblatt, M.; Groult, D. *J. Phys. IV* **1993**, *3*, 133−136.

(45) Ottolenghi, A.; Foury, P.; Pouget, J. P.; Teweldemedhin, Z. S.; Greenblatt, M; Groult, D.; Marcus, J.; Schlenker, C. *Synth. Met.* **1995**, *701*, 1301−1302.

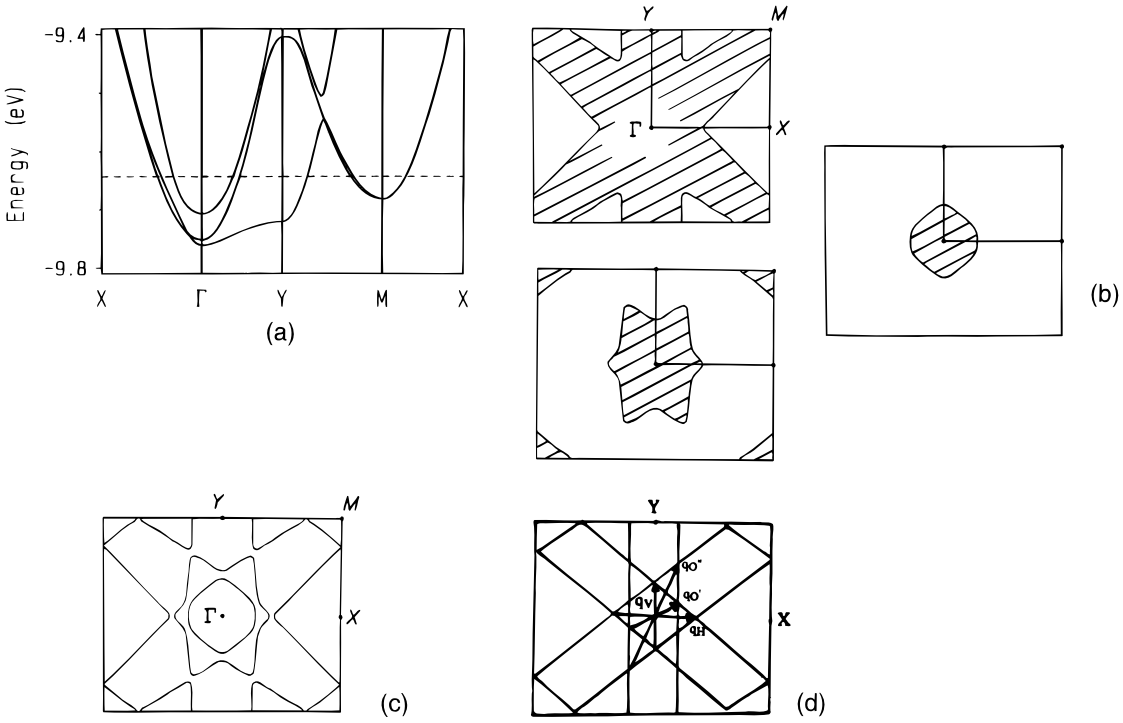

Figure 11. (a) Dispersion relations of the bottom portion of the t_{2g} block bands calculated for the W_6O_{22} slab of $P_4W_{12}O_{44}$ where the dashed line is the Fermi level corresponding to 2d-electrons per unit cell; Γ = (0, 0), X = (a*/2, 0), Y = (b*/2, 0), Z = (0, c*), and M = (b*/2, c*/2). (b) Fermi surfaces of the three partially filled bands of $P_4W_{12}O_{44}$. (c) Combined Fermi surfaces of $P_4W_{12}O_{44}$. (d) Hidden 1D nesting Fermi surfaces in $P_4W_{12}O_{44}$. Reprinted with permission from ref 5. Copyright 1989 American Institute of Physics.

unambiguous transitions to CDW states. Analysis of the X-ray data confirms that these fluctuations can be associated with modulations of three sets of infinite chains of WO_6 octahedra running along the a, $a + b$, and $a - b$ directions in the ReO_3-type infinite layers in these materials. The leading instability changes from the chain along a for the $m = 4$ member to chains along $a \pm b$ for larger values of m. In the $m = 4$ and 6 bronzes the observed **q**, CDW satellite reflections correspond to a single wave vector modulation that simultaneously nests two differently oriented 1D FSs associated with these chains (e.g., $\mathbf{q}_H$ in Figure 11d), thereby gaining a maximum of electronic energy; the quasi-1D FSs associated with these chains correspond to two hidden 1D FSs in Figure 11d.[42−45]

For the $m = 4$ and 6 members the CDW instabilities are incommensurate. Moreover, results of Hall measurements and observation of large anisotropic magnetoresistance effects in the low-temperature state of the $m = 4$ and 6 phases support the presence of electron and hole pockets with high mobility.[40] These latter data are confirming evidence of quasi-cylindrical FSs and partial opening of a gap at the FS at T_c in the 2D MPTBs. The $m = 7$ phase also undergoes at least two successive CDW modulations. However, they differ in many respects from those exhibited by the $m = 4$ and 6 members. First, the XRDS studies show that the modulations, at both T_{c1} and T_{c2}, are not sinusoidal, since several harmonics of the fundamental wave vector are detected.[43] Second, the temperature dependence of both the resistivity and the CDW satellite intensity at T_{c1} shows hysteresis, which is indicative of a structural transition closer to first order than second order. These phenomena may be due to strong electron−phonon coupling and may be explained with a bipolaron-type model.[40] Alternatively, strong electron−electron interactions can lead to localization of a fraction of the carriers below T_{c1}, possibly along one of the three chains only, by a process similar to a Wigner crystallization.[43] The origin of the low-temperature transition (i.e., at 47 K) in the $m = 7$ sample is not clear at present. The $m = 8$ member does not show any long-range order down to $T = 35$ K, but condensation of diffuse scattering corresponding to short-range order is observed for two different commensurate modulations ($\mathbf{q}_1$ and $\mathbf{q}_2$) at $T_{c1} = 220$ K and $T_{c2} = 200$ K. Two successive structural phase transitions have been observed for the $m = 9$ phase at $T_{c1} \approx 445$ K, leading to a doubling of the unit cell ($\mathbf{q}_1 = a$*/2), and $T_{c2} = 324$ K, a modulation corresponding to a tripling of the previously modulated supercell ($\mathbf{q}_2 = 1/3a$*). Single-crystal X-ray diffraction patterns taken only at room temperature of the $m = 10$ and 12 phases show commensurate modulation wave vectors corresponding to structural transitions. Whether or not these structural transitions in the $m \geq 8$ phases are associated with CDW electronic instabilities and FS nesting is not established as yet.[45] The transition temperatures obtained from the resistivity and XRDS measurements are collected in Table 1 along with crystal data, room-temperature resistivity, and the average formal valence of W for each compound.

Both T_{c1} and T_{c2} (with the exception of $m = 4$ and 6) increase with increasing m or layer thickness (Table 1). This is consistent with increased low dimensionality, which favors better FS nesting for higher m and therefore an increased stability of the CDW state. Bond-valence-sum analysis of these phases indicates that the 5d-electrons are primarily located in the middle of the WO_6 blocks.[46] Hence, the interlayer coupling along the c direction is expected to decrease with increasing m. On the other hand, the electrical resistivity seems to increase with m in the whole range

(46) Domenges, B.; McGuire, N. K.; O'Keefe, M. *J. Solid State Chem.* **1985**, *56*, 94−100.

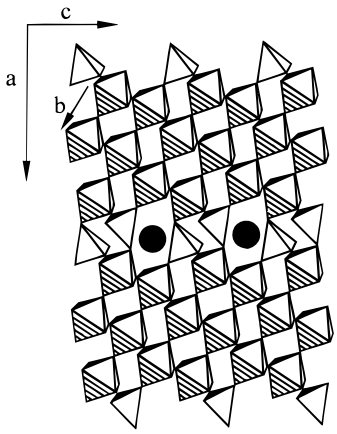

Figure 12. Schematic structure of the monophosphate tungsten bronzes, $A_x(PO_2)_4(WO_3)_{2m}$, with the A cations (solid circles) in the hexagonal tunnels $MPTB_h$ ($m = 6$).

of temperature. This behavior is probably related to the decreasing number of charge carriers with increasing m (i.e., the number of 5d-electrons per W is $2/m$), which can lead to a decrease of screening and larger intralayer electron−electron repulsions and/or to stronger electron−phonon interactions.

Monophosphate Tungsten Bronzes with Hexagonal Tunnels

Structure. The $MPTB_h$s, $A_x(PO_2)_4(WO_3)_{2m}$ form with A = Na and K; the value of x depends on A, and m and ranges between 1.75 and 3. Compounds with m from 4 to 13 have been prepared.[28,30] The structures of $MPTB_h$s are closely related to those of $MPTB_p$s; corner-sharing WO_6 slabs of ReO_3-type are connected through PO_4 planes. At the juncture between two octahedral layers, the octahedra and tetrahedra corner-share to form hexagonal tunnels (Figure 12) where the A cations are located. The structure of the $m = 4$ member of $A_x(PO_2)_4(WO_3)_{2m}$ is similar to that of η-Mo_4O_{11}, with PO_4 replacing the MoO_4 tetrahedra at the edges of the ReO_3-like blocks.[47] The structures of $MPTB_h$s differ from those of $MPTB_p$s by the relative orientation of the layers. In $MPTB_p$s the octahedra strings exhibit a zigzag configuration (Figure 4), while in $MPTB_h$s, the strings of octahedra remain parallel from one ReO_3-type layer to the next (Figure 12).

Large (~6 × 3 × 0.8 mm^3), purple, platelike, monoclinic single crystals of $Na_2P_4W_{12}O_{44}$ were obtained in the hot zone, by heating a polycrystalline sample of the same composition to 1050 °C for 1 week and slowly cooling it to room temperature in ~2 weeks. Similarly, copper-colored, platelike crystals of $Na_xP_4W_8O_{32}$ with $x = 1.3$ and 1.6 with an average size of ~4 × 1.5 × 0.8 mm^3 were obtained from an $Na_2P_4W_8O_{32}$ composition.[48]

Physical Properties. The temperature variation of resistivity for $Na_2P_4W_{12}O_{44}$ and $Na_{1.6}P_4W_8O_{32}$ show metallic and quasi-2D behavior. The anisotropy is greater in $Na_2P_4W_{12}O_{44}$ than in $Na_{1.6}P_4W_8O_{32}$ by about an order of magnitude. A weak and broad metal-to-metal transition is seen in $Na_2P_4W_{12}O_{44}$ at ~140 K along both a^* (hard direction of conductivity) and b (easy direction of conductivity) (Figure 13). In $Na_{1.6}P_4W_8O_{32}$ the metal-to-metal transition is weaker, but

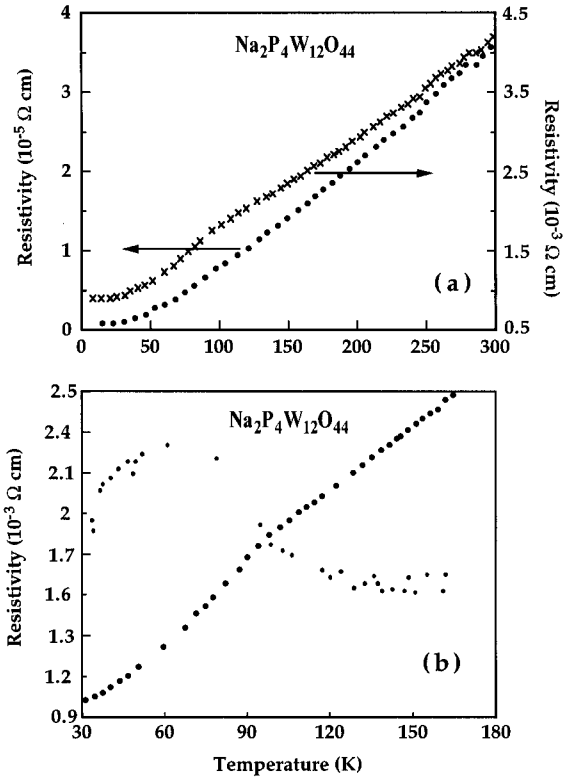

Figure 13. (a) Temperature dependence of the resistivity for $Na_2P_4W_{12}O_{44}$ along b (●) and a^* (×) axes. (b) An expanded view of the resistivity transition along b (●) and $d\rho/dT$ (•). Reprinted with permission from ref 48. Copyright 1989 Academic Press.

observable at ~90 K along the b direction. The magnetic susceptibility measurements are consistent with the resistivity data and show Pauli-paramagnetic behavior for both $MPTB_h$s and large drops in the susceptibility at ~150 and ~100 K for $Na_2P_4W_{12}O_{44}$ (Figure 14) and $Na_{1.6}P_4W_8O_{32}$, respectively.

To a first approximation, the d-block band electronic structure of the $MPTB_p$s and $MPTB_h$s would be expected to be similar, except for the number of electrons filling the band. This was confirmed by calculations of the band structure by the EHTB method.[27] Comparison of the band structures of $P_4W_8O_{32}$ and $P_4W_{12}O_{44}$ with those of $Na_{1.6}P_4W_8O_{32}$ and $Na_2P_4W_{12}O_{44}$ show that the dispersions of the bottom t_{2g} bands are similar in the $MPTB_p$s and $MPTB_h$s with the same m value. The FSs calculated for the $MPTB_h$s are similar to those shown in Figure 11 with hidden, 1D well-nested FSs. Thus, the weak anomalies seen in the resistivity and magnetic susceptibility of the $MPTB_h$s are likely due to CDW instabilities. X-ray scattering experiments are underway to confirm this hypothesis.

The multiple resistivity anomalies of the $MPTB_p$s, which have been confirmed to be due to CDW instabilities, are much more pronounced than those observed in the $MPTB_h$s. Analysis of the W−O band orbitals by Canadell and Whangbo have shown that their partially filled bands are represented by the orbitals of all the WO_6 octahedra including those at the surfaces of the W−O layers. Thus, CDW formation in the $MPTB_h$ layers may be hindered and/or prevented by random potentials created by disordered cations in the hexagonal channels; this effect could account for the weaker anomaly seen in the $MPTB_h$s compared with that in $MPTB_p$s.[27]

(47) Kihlborg, L. *Ark. Kemi* **1963**, *21*, 365−377.
(48) Wang, E.; Greenblatt, M.; Rachidi, I. E.-I.; Canadell, E.; Whangbo, M.-H. *J. Solid State Chem.* **1989**, *81*, 173−180.

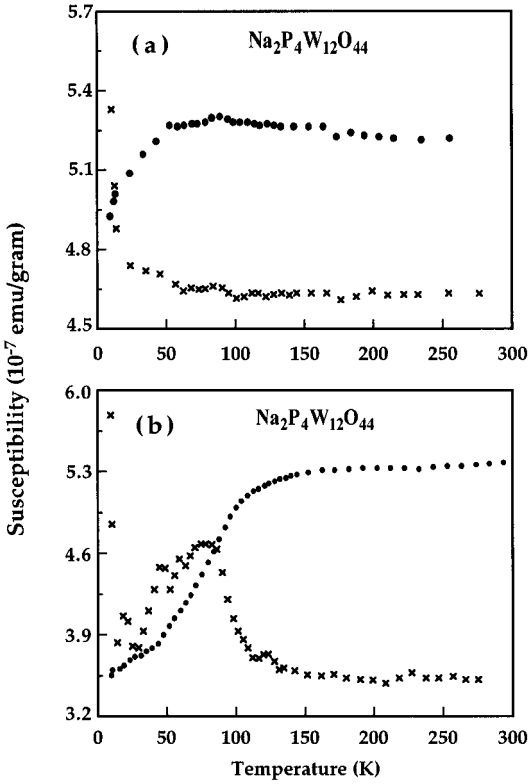

Figure 14. (a) Temperature dependence of the magnetic susceptibility χ vs T (●) and dχ/dT (×) with **H** in the *bc* plane. (b) χ vs T (●) and dχ/dT (×) with **H** parallel to a^* (hard direction) for $Na_2P_4W_{12}O_{44}$. Reprinted with permission from ref 48. Copyright 1989 Academic Press.

Other Phosphate Tungsten Bronzes. The synthesis and characterization of the other classes of PTBs including the DPTBs $CsP_8W_8O_4$ and $P_8W_{12}O_{52}$ have been recently reviewed.[32]

Conclusion

The homologous series of monophosphate tungsten bronzes $(PO_2)_4(WO_3)_{2m}$ ($MPTB_p$) and $A_x(PO_2)_4(WO_3)_{2m}$ ($MPTB_h$) have structural and electronic features in common with the quasi-2D $A_{0.9}Mo_6O_{17}$ molybdenum bronzes. In these materials the metal−oxygen (M−O) layers are made up of ReO_3-type MO_6 (Mo, W) corner-sharing octahedra. In the Mo bronzes, the LD properties and the associated CDW instability observed are the result of the separation of the Mo−O layers by the A cations and the preferential delocalization of the unpaired electrons along certain 1D chains of MoO_6 octahedra within the ReO_3-like blocks. Similarly, the origin of LD behavior of the MPTBs is the separation of the conducting ReO_3-like W−O blocks by the phosphate groups, and here again, the unpaired electrons are found primarily on 1D chains of WO_6 within the ReO_3-type blocks. The 2D Mo bronzes exhibit a single CDW-driven instability. One of the signatures of this CDW shows up as a sigmoidal-shaped MMT in the temperature dependence of the electrical resistivity. The $MPTB_p$s, for $m = 4$, 6, and 7, indicate two such CDW transitions. Band structure calculations by Canadell and Whangbo have shown in detail how the three dispersive, partially filled bottom t_{2g} block bands in these materials lead to hidden, nesting, 1D FSs, which account for the observed CDW transitions. X-ray diffraction experiments by Pouget et al. have shown that the nesting mechanism of the FSs, which leads to the CDW state and the observed superlattice reflections at T_{c1} and T_{c2}, is correlated with modulations involving three infinite WO_6 chains, which give rise to the hidden, 1D FSs predicted by the band calculations of Canadell and Whangbo. It is noteworthy that the $m = 2$ and $m > 7$ members of the $MPTB_p$ series are semiconducting and follow Curie−Weiss behavior in their magnetic properties; it appears that the two electrons/W−O layer become localized in narrow bands for values of $m = 2$ and $m \geq 8$. In general, the electrical resistivity increases with increasing m and T_{c1} and T_{c2} increase with increasing m as well. These observations are consistent with the structural properties which lead to increasing low dimensionality and decreasing carrier concentration and screening with increasing m.

The analogous $MPTB_h$ compounds with $m = 4$ and 6, $Na_{1.6}P_4W_8O_{32}$ and $Na_2P_4W_{12}O_{44}$, only studied by electrical conductivity and magnetic susceptibility measurements so far, exhibit a single, weak anomaly, presumably related to a CDW transition. Diffraction studies are required to show that these transitions are unambiguously related to CDW instabilities, and if they are, how they correlate with modulations of the corresponding WO_6 chains.

This work would not have been possible without the many contributions of my students, especially Dr. B. Collins, who worked on the Mo bronzes, and Dr. E. Wang, who was the first to grow large single crystals of the various PTBs and made the first discoveries of cascading CDWs in some of these phases. My student Dr. Z. S. Teweldemedhin continued to grow large single crystals of PTBs and explored carefully the effect of the width of the ReO_3-type slabs on the electronic transport and other physical properties. Dr. K. V. Ramanujachary, a Research Associate and now an Assistant Professor at Rowan College, NJ, always contributes to every project by knowing how to grow crystals and measure critical properties accurately and thinking about the interpretations critically. Emeritus-Professor W. H. McCarroll of Rider College is another colleague who contributes substantially to nearly every aspect of my research. Band calculations by Professors E. Canadell of the Universite de Paris-Sud, M.-H. Whangbo at North Carolina State University, and their graduate students helped immensely in the understanding of our experimental results. Finally collaborations with Professor J. P. Pouget and his students of the Universite de Paris-Sud, who found unambiguous evidence of the CDW state by diffuse X-ray scattering experiments in the MPTBs, and with Professor C. Schlenker and her associates of the CNRS and Universite Joseph Fourier de Grenoble, whose detailed magnetotransport measurements helped further elucidate the electronic structure of these materials, is gratefully acknowledged. This work was supported by the National Science Foundation-Solid State Chemistry Grant DMR-93-14605.

AR950157+